Neurobiology of Disease 227 (2026) 107516

Contents lists available at ScienceDirect

Neurobiology of Disease

journal homepage: www.elsevier.com/locate/ynbdi

Evidence for hippocampal globotriaosylceramide (Gb3) accumulation and spatial memory impairment in a mouse model of Fabry disease

Marco Salluzzo [a], Francesca Flotta [b], Cecilia Delprete [c,d], Violetta Lazzarotti [a], Francesco Formaggio [d], Beatrice Vignoli [e], Ludovica Campolongo [d], Gabriele Campana [d], Lucia Carboni [d], Marco Canossa [f], Vincenzo Donadio [b,c], Rocco Liguori [b,c], Marco Caprini [c,d,**], Roberto Rimondini [a,*]

[a] Department of Medical and Clinical Sciences (DIMEC), University of Bologna, Italy
[b] Department of Biomedical and Neuromotor Sciences (DIBINEM), University of Bologna, Italy
[c] IRCCS Istituto delle Scienze Neurologiche di Bologna, Bologna, Italy
[d] Department of Pharmacy and Biotechnology (FaBiT), University of Bologna, Italy
[e] Institute of Neuroscience, National Research Council, Padova Section, 35131 Padova, Italy
[f] Department of Cellular, Computational and Integrative Biology - CIBIO, University of Trento, Povo, Italy

ARTICLE INFO

Keywords:
Fabry disease
Globotriaosylceramide (Gb3)
α-Gal A(-/0) mouse model
Neuron
Astrocyte
Microglia
Spatial memory
Morris water maze

ABSTRACT

Fabry disease (FD) is an X-linked lysosomal storage disorder caused by pathogenic variants in the GLA gene that reduce α-galactosidase A activity and lead to progressive accumulation of globotriaosylceramide (Gb3) and related glycosphingolipids. In the human brain, Gb3 deposition is reported predominantly within the endothelium of small cerebral vessels and is associated with cerebrovascular dysfunction, seizures, cognitive impairment, and neuropsychiatric symptoms. In experimental animal models, its regional distribution, cellular localization, and relationship to cognitive dysfunction remain incompletely defined and appear to vary according to species, model, age, disease severity, and detection method.

Here, using the α-galactosidase A hemizygous knockout mouse (α-Gal A −/0) and immunofluorescence, we performed a regional and cell-type-specific characterization of Gb3 immunoreactivity in the hippocampus and assessed hippocampal-dependent spatial learning and memory. Compared with wild-type controls (α-Gal A +/0), α-Gal A −/0 mice showed a marked increase in hippocampal Gb3 immunoreactivity, with deposits localized mainly to vascular endothelial cells and frequent signal within the capillary lumen. Neuronal Gb3 signal was detected in dentate gyrus hilar neurons with mossy cell-like morphology. Gb3 did not overlap with astrocytic (GFAP) or microglial (Iba1) markers, although astrocytic endfeet and activated microglia were often apposed to Gb3-positive vessels. In parallel, α-Gal A (−/0) mice displayed impaired Morris water maze acquisition and reduced spatial memory during the probe trial, without changes in swimming speed or distance. These data suggest that α-Gal A deficiency is associated with increased hippocampal Gb3 immunoreactivity, mainly in neurovascular compartments, and with measurable impairment in spatial memory.

1. Introduction

Fabry disease (FD; OMIM: 301500) is an X-linked metabolic disorder caused by variants in the GLA gene (Xq22)(OMIM: 300644) that reduce the activity of α-galactosidase A (α-Gal A; EC 3.2.1.22) and lead to lysosomal accumulation of globotriaosylceramide (Gb3) and its deacylated derivative globotriaosylsphingosine (lyso-Gb3) in multiple tissues, including kidney, heart, and the nervous system (Cortés-Saladelafont et al., 2023; Germain, 2010; Ranieri et al., 2016; Tuttolomondo et al., 2024). Clinically, FD is a multisystem disease characterized by neuropathic pain, angiokeratomas, corneal verticillata, hypohidrosis, and progressive renal and cardiac involvement (Perrot

* Corresponding author at: Department of Medical and Clinical Sciences (DIMEC), University of Bologna, Via Irnerio 48, 40126 Bologna, Italy.
** Corresponding authors at: Laboratory of Cellular and Molecular Physiology, Department of Pharmacy and Biotechnology, Via S. Donato 19/2, 40127 Bologna, Italy.
E-mail addresses: m.caprini@unibo.it (M. Caprini), roberto.rimondini@unibo.it (R. Rimondini).

https://doi.org/10.1016/j.nbd.2026.107516
Received 16 April 2026; Received in revised form 19 June 2026; Accepted 29 June 2026
Available online 30 June 2026

et al., 2002; Wallace and Cooper, 1965). Central nervous system manifestations are common and are often attributed to cerebral small-vessel disease, including white matter abnormalities, lacunar infarcts, and ischemic stroke, which are thought to arise primarily from vascular substrate deposition and endothelial dysfunction (Altarescu et al., 2005; Buechner et al., 2008; Crutchfield et al., 1998; Grewal and Grewal, 1994; Hilz et al., 2004; Lidove et al., 2006; Mitsias and Levine, 1996; Moore et al., 2007, 2002). Neuropsychological and psychiatric symptoms - including cognitive impairment, depression, and anxiety - have also been reported, although their relationship to vascular pathology, pain burden, and potential direct parenchymal involvement remains complex (Bolsover et al., 2014; Laney et al., 2010; Loeb et al., 2018; Mroczek et al., 2022; Ohsawa et al., 2024; Sigmundsdottir et al., 2014).

Post-mortem support brain involvement in FD, including reports of Gb3 inclusions in vascular cells and, in some cases, glia and neurons in selected regions such as hippocampus (Kaye et al., 1988), neuronal hydropic swelling related to glycolipid deposition in the amygdaloid body and subiculum, without clear dentate gyrus hilar involvement (Okeda and Nisihara, 2008). In line with these this heterogeneity, MRI studies have reported reduced hippocampal volume in male Fabry patients, without a direct correlation with significant memory impairment (Fellgiebel et al., 2012). Because of the above-mentioned evidence, hippocampal pathology in FD should be interpreted as regionally and clinically heterogeneous rather than uniform across patients.

In animal models, the situation is also heterogeneous. Experimental models have been invaluable for mechanistic studies, yet FD rodent models do not consistently reproduce the human CNS phenotype, and the distribution of Gb3 in brain is variable across models, ages, and detection methods (Cortés-Saladelafont et al., 2023; Elsaid et al., 2022; Jabbarzadeh-Tabrizi et al., 2020; Miller et al., 2020, 2016; Ohshima et al., 1997; Taguchi et al., 2013). Species differences in glycosphingolipid metabolism may further contribute to discrepancies in Gb3 isoform composition and tissue distribution, potentially limiting translational relevance (Celi et al., 2022). An additional translational limitation is that α-Gal A-deficient mouse models do not reproduce the clinical distinction between classic and late-onset FD (Bangari et al., 2015; Germain, 2010; Nance et al., 2006). Therefore, findings obtained in the α-Gal A (−/0) model should be interpreted as mechanistic consequences of α-Gal A deficiency rather than as a direct correlate of all human Fabry phenotypes. Furthermore, it remains necessary to clarify whether such deposits are sufficient to disrupt hippocampus dependent cognitive functions. Addressing this issue is essential to distinguish the real limitations of the model from methodological variability in detecting brain glycosphingolipids and to establish whether local cellular distribution rather than overall substrate load is a determining factor of cognitive vulnerability in FD. In α-Gal A (−/0) mice, Gb3 accumulation is robust in peripheral tissues and sensory ganglia (Lakomá et al., 2016, 2014; Masotti et al., 2019; Obata, 2010), while brain findings range from vascular wall deposits with limited neuronal involvement (Itoh et al., 2001) to reports of behavioral and transcriptional alterations associated with hippocampal dysfunction in transgenic or sensitized models (Bangari et al., 2015; Kummer et al., 2025, 2018; Taguchi et al., 2023). Noteworthy, distinct dysregulations in the expression of neuropeptide genes and proteins were observed in the dynorphinergic, nociceptinergic and CRFergic systems of the prefrontal cortex, amygdala and thalamus of male and female α-Gal A (−/0) mice (Rullo et al., 2021). Behavioral and molecular alterations involving brain regions relevant to cognition and affect have also been reported in Fabry mouse models (Hofmann et al., 2017; Kummer et al., 2025, 2018). Therefore, the unresolved issue is not whether Gb3 accumulation can occur, but whether the commonly used α-Gal A (−/0) mouse shows hippocampal Gb3 immunoreactivity at defined cellular sites and whether this is associated with hippocampal-dependent behavioral impairment.

Based on these considerations, the present study was designed to test the hypothesis that α-Gal A deficiency is associated with hippocampal Gb3 immunoreactivity in anatomically defined cellular compartments and with impairment in hippocampal-dependent spatial memory. Specifically, we aimed to: (i) quantify Gb3 immunoreactivity in the hippocampus of α-Gal A (−/0) mice compared with α-Gal A (+/0) littermate controls; (ii) define the relationship of Gb3-positive signal to endothelial, neuronal, astrocytic, and microglial markers using confocal microscopy and orthogonal *Z*-stack analysis; and (iii) assess spatial learning and memory using the Morris water maze test. This focused experimental design was not intended as a systematic review of CNS Gb3 distribution, but rather as a cellular-resolution analysis of hippocampal involvement in a widely used mouse model of FD.

2. Material and methods

2.1. Animals

Heterozygous female α-Gal A (+/−) and wild-type (WT) α-Gal A (+/0) male mice (JAX strain B6; 129Gla-^{tm1Kul}/J) were purchased from Charles River Laboratories Italia s.r.l. (Jackson Laboratory, Bar Harbor, ME, USA) and crossed to generate offspring as previously described (Ohshima et al., 1997). Breeding was continued to obtain hemizygous knockout males (α-Gal A (−/0)) and male littermate controls (α-Gal A +/0) on a stabilized mixed B6;129 background. Only male mice were included to avoid variability related to X-chromosome inactivation and because FD tends to be more severe in males, although severity can vary among individuals (Biegstraaten et al., 2011; Juchniewicz et al., 2018; Lakomá et al., 2014).

Mice were housed in groups of up to six in individually ventilated cages (Tecniplast, Varese, Italy) with food and water available ad libitum under controlled environmental conditions (12 h light/dark cycle, lights on 07:00–19:00; 22 ± 2 °C; 65% humidity). Behavioral experiments were carried out at the Department of Medical and Clinical Sciences (DIMEC), University of Bologna, in agreement with national regulations. All procedures complied with European Community Council Directive 86/609/EEC and were approved by the Ethical Committee of the University of Bologna (Veterinary Service, protocol N. 141/2019PR). All experiments were performed on 12–18-month-old animals (total $n = 28$).

2.2. Immunohistochemistry

Animals were deeply anesthetized and perfused transcardially with 4% paraformaldehyde (PFA; Sigma) in phosphate-buffered saline (PBS; 0.01 M, pH 7.4). Brains were post-fixed overnight in 4% PFA, transferred to PBS, and stored at 4 °C until processing. Coronal sections (30 μm) were cut using a Leica VT1000S vibratome and stored in PBS.

To reduce tissue autofluorescence, free-floating sections underwent a photobleaching protocol (Sun et al., 2017). Briefly, sections were placed in PBS (1 mL/well) in a multiwell plate and exposed to white LED light for 48 h at 4 °C.

Sections were then subjected to antigen retrieval by incubation in sodium citrate buffer (10 mM sodium citrate, pH 6.0 and 10 mM Tris-HCl, pH 6.0) for 5 min at room temperature, followed by heating at 85 °C for 10 min and cooling on ice for 5 min. After four PBS washes (10 min each), sections were blocked for 1 h at room temperature in PBS containing 10% normal goat serum (NGS; Abcam) and 3% Triton X-100. Primary antibodies (Table 1) were diluted in PBS containing 1% NGS and 2% Triton X-100 and incubated overnight at 4 °C with gentle agitation. The next day, sections were washed (4 × 10 min PBS) and incubated for 2 h at room temperature with appropriate secondary antibodies (Table 1) diluted in the same buffer, protected from light. Sections were then washed (4 × 10 min PBS), counterstained with DAPI (5 min), mounted on glass slides, and coverslipped with Vectashield® mounting medium.

For all immunofluorescence experiments, α-Gal A (+/0) control sections were processed in parallel with α-Gal A (−/0) sections using

Table 1
Antibodies used for immunohistochemistry.

Antibody	Dilution rate	Seller company
Mouse Monoclonal Anti-Gb3	1:100	TCI Chemicals (A2506)
Rabbit Anti-ERG	1:100	Abcam (ab92513)
Rabbit Anti-NeuN	1:400	Cohesion Biosciences (CQA1012)
Polyclonal Rabbit Anti-GFAP	1:400	Agilent (Z033429–2)
Recombinant Monoclonal Rabbit Anti -AIF1/IBA1	1:500	ABclonal (A19776)
Polyclonal Rabbit Anti-CD31/PECAM1	1:100	ABclonal (A0378)
Anti-PGP9.5 antibody [EPR4118] - Neuronal Marker	1:1000	Abcam (AMab 108,986
CY3-conjugated AffiniPure Goat Anti-Mouse IgG (H + L)	1:1000	Jackson Immunoresearch Laboratories (AB_2338680)
Alexa Fluor 488-conjugated Donkey Anti-Rabbit IgG	1:1000	ABCAM (ab150065)
DAPI for nucleic acid staining	1:1000	Sigma Aldrich (D9542-10MG)

identical antibody concentrations, incubation times, imaging settings, and post-acquisition parameters. Because lipid immunodetection can be influenced by antibody specificity, fixation, antigen retrieval, and tissue processing, the signal detected with the anti-Gb3 antibody is referred to throughout the manuscript as "Gb3 immunoreactivity" or "Gb3-positive signal" unless otherwise specified. The present study did not include an independent anti-Gb3 antibody, staining for an additional lipid species, or biochemical quantification of Gb3 isoforms and lyso-Gb3 in microdissected hippocampal tissue. These points are acknowledged as limitations, particularly because lipidomic studies have shown that Gb3 species and lyso-Gb3 can vary by model, genotype, tissue, and disease severity (Jabbarzadeh-Tabrizi et al., 2020; Taguchi et al., 2023), and because lyso-Gb3 is widely used as a FD biomarker and has potential biological activity (Nikolaenko et al., 2023; Ramaswami et al., 2025).

Table 1. Dilution, description, and supplier information for antibodies used in immunohistochemistry.

2.3. Image acquisition and analysis

Images were acquired using a Nikon A1-R+ confocal laser scanning microscope equipped with 401.9, 489.3, and 561 nm laser lines to excite DAPI (blue), Alexa Fluor 488 (green), and Cy3 (red), respectively. Images were collected at multiple magnifications using a Nikon 20× (NA 0.75), 60× (NA 1.4), and 100× (NA 1.45) objective. Emission signals were detected by a photomultiplier tube (DU4) with band-pass filters (450/50 nm, 525/50 nm, and 595/50 nm for DAPI, Alexa Fluor 488, and Cy3, respectively). For quantitative Gb3 fluorescence intensity measurements, *Z*-stacks were acquired using identical microscope settings across experiments (DAPI: HV 214, offset −5, laser 0.35; Cy3: HV 90, offset −26, laser 0.45). Acquisition and initial processing were performed using Nikon NIS-Elements AR-2 (Nikon Inc., USA). Mean intensities were computed on maximum-intensity projections using Fiji (Schindelin et al., 2012). Colocalization was assessed qualitatively by inspection of Z-stacks and orthogonal views using NIS-Elements AR-2 and NIS-Elements Viewer 5.21. Given the punctiform, compartmentalized, and largely non-overlapping nature of Gb3-positive structures, colocalization was assessed qualitatively on complete Z-stacks and orthogonal views rather than using Pearson or Manders correlation coefficients, which could underestimate the data in cases of diffuse or discontinuous distribution.

2.4. Morris water maze test

Mice were trained in the Morris water maze (MWM) to locate a hidden escape platform using a protocol adapted from previous work (Stagni et al., 2016) and based on established procedures (Vorhees and Williams, 2006). The apparatus consisted of a circular pool (1.00 m diameter, 50 cm height) filled with water maintained at 22 ± 1 °C and rendered opaque with milk. A transparent circular platform (10 cm diameter) was submerged 0.5 cm below the water surface and maintained in a fixed position (center of the southwest quadrant). The pool was located in a room containing both intra-maze and extra-maze visual cues. On day 1, mice received one session of three trials. On days 2–5, mice received two sessions of three trials per day (inter-session interval 45 min). Each trial started with the mouse placed into the pool facing the wall from one of four starting points (north, east, south, west) and lasted up to 60 s. If the platform was not located within 60 s, the mouse was guided to the platform and allowed to remain there for 15 s. Inter-trial interval was 10 s in a holding cage. During acquisition, escape latency time, swim speed, path length and proximity were analyzed. Retention was assessed with one trial (probe trial), on the sixth day, 24 h after the last acquisition trial, using the same starting point for all mice. Mice were allowed to search for up to 60 s for the platform. For the probe trial, the total time spent in the former platform quadrant, the frequency of crossing the former platform, the proximity to the former platform position (Gallagher's test), the swimming speed and the percentage of time spent in each quadrant were employed as measures of retention of acquired spatial preference. All experimental sessions were carried out between 9.00 am and 5.00 pm. Behavior was recorded with a camera mounted above the pool and analyzed using EthoVision XT® (v15; Noldus). During acquisition, escape latency and swim speed were analyzed.

2.5. Sample size and power considerations

Sample size was based on the availability of age-matched α-Gal A (−/0) and α-Gal A (+/0) male littermates and was consistent with previous behavioral and histological studies using FD mouse mode and established MWM protocols in mice. A two-sided sensitivity analysis was performed to estimate the minimum detectable effect size for the available cohorts at $\alpha = 0.05$ and 80% power. Sensitivity analyses were performed using G*Power, following established procedures for statistical power analysis (Faul et al., 2007). For the MWM cohort, $n = 14$ mice per genotype provided 80% power to detect a large genotype effect of approximately Cohen's $d = 1.10$ in two-group comparisons. For immunofluorescence analyses, $n = 6$ animals per genotype provided 80% power to detect large genotype effects of approximately Cohen's $d = 1.80$–1.91, depending on the exact group size. Therefore, the study was powered to detect robust genotype-dependent behavioral and histological differences, whereas smaller effects may require larger confirmatory cohorts.

2.6. Statistical analysis

Experimental data were analyzed using GraphPad Prism (v8.0). Normality and homogeneity of variance were assessed using the Shapiro-Wilk and Levene's tests, respectively. Normally distributed data are presented as mean ± SEM. A significance threshold of $p \leq 0.05$ was used.

Gb3 fluorescence intensity was quantified from four *Z*-stack acquisitions of three comparable hippocampal sections per animal. Z-stacks were converted to maximum-intensity projections prior to measurement. Gb3 Z-stacks were converted to maximum-intensity projections before measurement. For each mouse, fluorescence intensity values from all analyzed Z-stack projections were averaged to generate one value per animal and group comparisons were performed using animal-level values using a two-tailed unpaired Student's *t*-test. Projection-level values were used only to derive the animal mean and are not reported as independent sample sizes. For two-group comparisons, normally distributed data with homogeneous variance were analyzed using a two-tailed unpaired Student's t-test.

Cell-type localization analyses were performed on one comparable hippocampal section per animal (approximately −1.70 mm from bregma) using four Z-stack acquisitions per section.

MWM learning-trial data (latency to platform, swim proximity to platform and velocity) were analyzed using a Repeated measure two-way ANOVA (Genotype as factor and day as repeated measure) followed by Tukey HSD post hoc test. Probe-trial outcomes (time in the former platform zone, Gallagher proximity test, latency to first entry into the former platform zone, frequency on former platform, total swim distance, and swim speed) were analyzed using two-tailed unpaired Student's *t*-tests. Sample sizes are reported in the figure legends.

3. Results

3.1. Hippocampal Gb3 immunoreactivity is increased in α-Gal A (−/0) mice

Coronal hippocampal sections from hemizygous α-Gal A (−/0) mice and α-Gal A (+/0) controls were processed by immunofluorescence to visualize Gb3 accumulation. Representative images show markedly increase in Gb3 signal in α-Gal A (−/0) than α-Gal A (+/0) animals (Fig. 1A, B).

Fluorescence intensity was first measured from multiple *Z*-stack projections per animal and then averaged to obtain one biological value per mouse. Statistical analysis was performed using these animal-level values only. α-Gal A (−/0) mice showed significantly higher

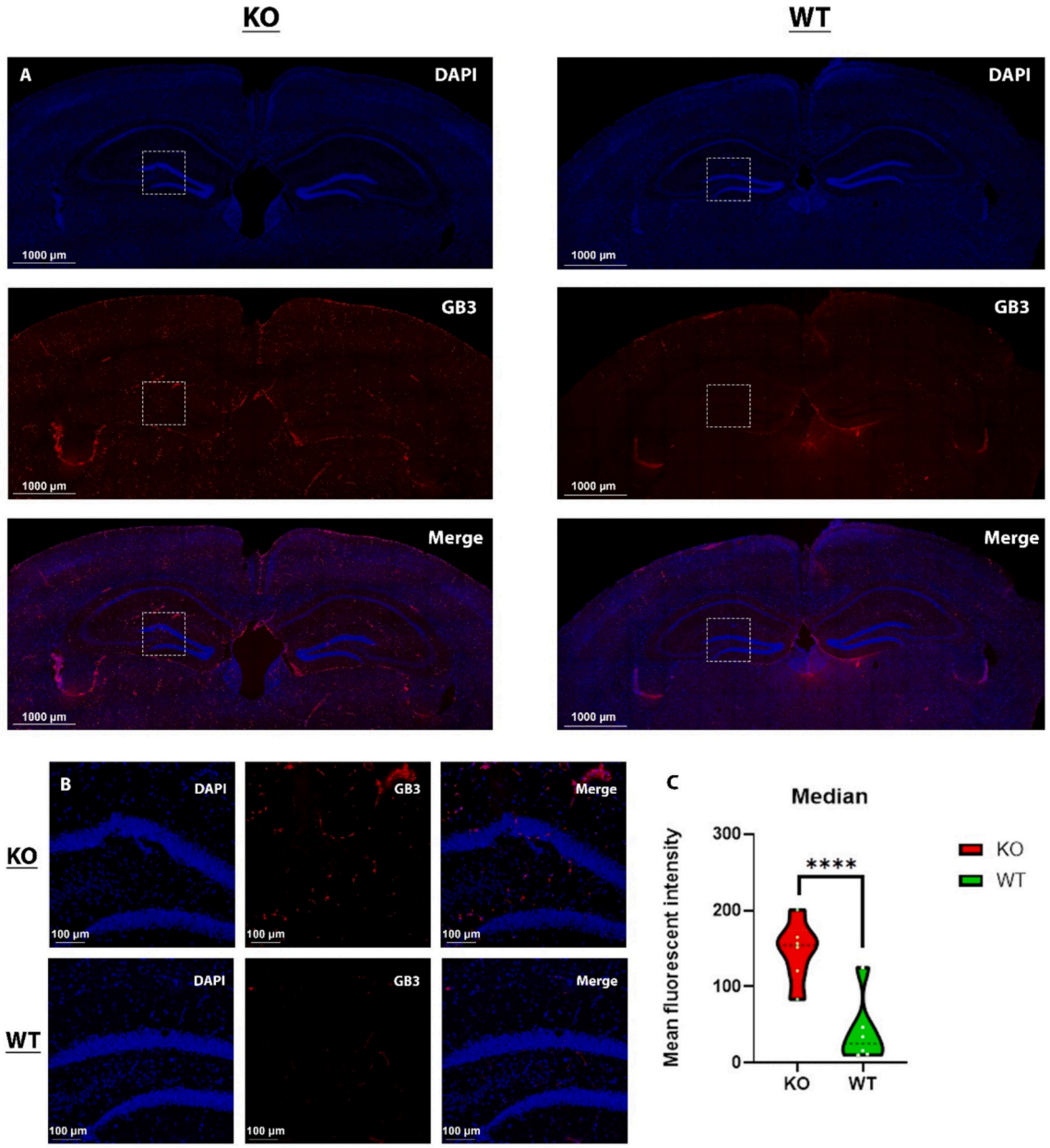

Fig. 1. Gb3 quantification in hippocampus. Immunohistochemistry for Gb3 was performed on the hippocampus of mice α -Gal A (−/0) or α-Gal A (+/0) for GLA. A: confocal microscope reconstruction (stitching of 2.5× magnification images) of a coronal section of the hippocampus (Bregma ≈ −1,70 mm) of a α-Gal A (−/0) (left) and α-Gal A (+/0) (right) mouse. B: high magnification (20×) of the region indicated by the white square in A. C: comparison of Gb3 immunoreactivity between α-Gal A (+/0) and α-Gal A (−/0) mice. Scale bars are indicated in the images. Data are presented as individual animal-level values with mean and SEM. Each point represents one animal, calculated from the average fluorescence intensity of multiple *Z*-stack projections. Groups were compared using a two-tailed unpaired Student's *t*-test. Statistical significance set at *p*-value <0,05; **** $p < 0.0001$. $n = 6$ per group.

hippocampal Gb3 immunoreactivity than α-Gal A (+/0) controls (α-Gal A (−/0) intensity = 146.5 ± 16.38 vs α-Gal A (+/0) Intensity = 43.85 ± 17.9, two tailed unpaired Student's *t*-Test $t = 4.362$, df = 10 $p < 0.0014$; $n = 6$ each genotype).

3.2. Gb3 immunoreactivity is detected in dentate gyrus hilar neurons of α-Gal A (−/0) mice

To determine whether hippocampal Gb3 signal is present in neurons, we performed double immunolabeling using two neuronal markers, PGP9.5 and NeuN, in combination with Gb3.

Double labeling for Gb3 and PGP9.5 (α-Gal (−/0): n = 6; α-Gal A (+/0): n = 6; 2–3 sections per animal) revealed Gb3-positive immunoreactivity associated with neuronal somata in the dentate gyrus hilus of α-Gal A (−/0) mice (Fig. 2A-C), whereas α-Gal A (+/0) sections showed only weak vascular signal without neuronal localization (Supplementary Fig. 1A, B). In α-Gal (−/0) mice, Gb3-positive neurons displayed morphology and branching consistent with mossy cells of the dentate gyrus polymorphic layer (Amaral et al., 2007). However, in the absence of specific molecular markers, neuronal heterogeneity within the hilar population cannot be excluded. For this reason, this anatomical assignment should be considered descriptive rather than definitive. Therefore, these neurons are referred to as hilar neurons with mossy cell-like morphology, and neuronal heterogeneity within the Gb3-positive hilar population cannot be excluded.

The Gb3 signal was not detected in neurons outside the dentate gyrus (data not shown). High-magnification confocal Z-stacks and three-dimensional reconstructions indicated that Gb3-positive structures were restricted to the soma (Fig. 2B, C). The Gb3-positive structures showed a reproducible polyhedral-like morphology with a central signal void; however, because this morphology was defined by immunofluorescence, its ultrastructural correlate remains to be established. Double immunoreactivity for Gb3 and NeuN showed no direct overlap between the two signals in hippocampal sections from either genotype (α-Gal (−/0): $n = 6$; α-Gal A (+/0): n = 6; 2–3 sections per animal), despite clear Gb3 aggregates (Fig. 2 D-F; Supplementary Fig. 1C, D). In the hippocampal regions examined, Gb3 puncta were adjacent to NeuN-positive somata but did not overlap with nuclear marker, indicating a possible intracellular compartment. Previous evidence has reported limited or regionally selective neuronal Gb3 immunoreactivity in FD models, supporting a cautious interpretation of cell-type localization (Itoh et al., 2001; Obata and Obrig, 2010).

3.3. Gb3 immunoreactivity does not overlap with astrocytic or microglial markers but is frequently associated with hippocampal microvessels

To assess whether Gb3 signal overlaps with astrocytes, sections were labeled for GFAP. Although Gb3 signal was more prominent in α-Gal (−/0) than α-Gal A (+/0) mice, no overlapping with GFAP was detected in either genotype (Fig. 3; Supplementary Fig. 3; α-Gal (−/0): $n = 6$; α-Gal A (+/0): n = 6; 2–3 sections per animal). Gb3-positive structures were frequently localized to hippocampal capillaries, and GFAP-positive astrocytic processes often wrapped these vessels, consistent with astrocytic endfeet contributions to the blood-brain barrier (Fig. 3A-F). Notably, the Gb3 signal was observed across the full diameter of some capillaries and within the vessel lumen (Fig. 3 B, C), suggesting that Gb3 immunoreactivity is not limited to the endothelial wall. Although intriguing, the presence of Gb3 within the capillary lumen must be interpreted with caution as it could reflect substrate circulation, endothelial leakage, altered clearance mechanisms, or antibody accessibility rather than a true "stable" intraluminal deposit.

Microglia were examined using Ionized calcium-binding adapter molecule 1 (Iba1) antibody (Imai et al., 1996). In α-Gal A (−/0) mice, numerous Iba1-positive cells displayed an activated morphology and processes oriented toward Gb3-positive vessels (Fig. 4 A-C). However, Gb3 signal did not overlap with Iba1, indicating that microglia are not a major storage compartment under these conditions. α-Gal A (+/0) sections showed minimal Gb3 signal and no microglial association (Supplementary Fig. 4; α-Gal (−/0) $n = 6$; α-Gal A (+/0): n = 6; 2–3 sections per animal).

Because colocalization was assessed by confocal *Z*-stacks observations and orthogonal views rather than by quantitative Pearson or Manders coefficients, these data should be interpreted as anatomical evidence of signal adjacency or non-overlap, rather than as a quantitative measure of molecular colocalization.

3.4. Endothelial-associated Gb3-positive structures within hippocampal microvessels in α-Gal A (−/0) mice

To test whether Gb3-positive structures are associated with hippocampal capillaries, sections were co-labeled with ERG and CD31. ERG was used to identify endothelial nuclei as ERG is a reliable endothelial nuclear marker in the CNS (Haber et al., 2015), whereas CD31/PECAM - 1 was used to delineate vessel profiles and endothelial cell border.

In α-Gal (−/0) mice, confocal Z-stacks showed Gb3 positive structures surrounding ERG-immunoreactive endothelial nuclei without ERG/Gb3 clear signal overlap (Fig. 5 A-C), indicating a perinuclear or cytoplasmic/organellar endothelial - associated localization. Gb3-positive structures were not observed in ERG-positive endothelial cells of α-Gal A (+/0) hippocampal sections (Supplementary Fig. 2 A-C; α-Gal (−/0): n = 6; α-Gal A (+/0): n = 6; 2–3 sections per animal).

Consistently, co-labeling with CD31 revealed that Gb3-positive signal aligned with the CD31-positive vessel wall in α-Gal (−/0) mice (Fig. 5 D, E). Three-dimensional reconstructions in orthogonal planes confirmed a pattern of Gb3-positive structures that followed the capillary wall and, in some cases, extended into the lumen. No comparable Gb3 positive deposition was detected in hippocampal vessels of α-Gal A (+/0) (Supplementary Fig. 2D-F; α-Gal (−/0): n = 6; α-Gal A (+/0): n = 6). These findings support endothelial-associated Gb3-positive structures within hippocampal microvessels in α-Gal A (−/0) mice.

3.5. Impairment of spatial learning and memory function in α-Gal A (−/0) mice

To test whether hippocampal Gb3 accumulation is associated with impaired spatial learning and memory, mice were evaluated in the MWM. During the 5-day acquisition phase, escape latency, swimming proximity to the platform zone and swimming velocity were measured. Compared with α-Gal A (+/0) controls, α-Gal A (−/0) mice showed a significant increase in escape latency [Repeated-measures two-way ANOVA main effect: day $F(4, 104) = 31.059$, $p < 0.0001$, genotype $F(1, 26) = 48.812$, $p < 0.0001$, genotype × day interaction $F(4, 104) = 0.765$, $p = 0.7419$]. Tukey's post hoc comparisons showed significant genotype differences on day 4 ($p = 0.002$), and day 5 ($p = 0.02$) (Fig. 6 A). With regards to swimming proximity to the platform zone, we observed a significant effect of day [$F(4,104) = 31.96$, $p < 0.0001$) and genotype [$F(1, 26) = 20.064$, $p < 0.00013$], with no significant genotype × day interaction [$F(4,104) = 1.66$, $p = 0.164$]. Tukey's post hoc comparisons showed significant genotype differences on day 4 ($p = 0.002$) and day 5 ($p = 0.02$) (Fig. 6 B). Furthermore, repeated 2-way ANOVA for swimming velocity during acquisition revealed a significant effect of day [$F(4,104) = 2691$, $p < 0.035$] and genotype [$F(1,26) = 33.658$, $p < 0.0001$], with no significant genotype × day interaction [$F(4,104) = 2.0198$, $p = 0.087$]. Tukey's post hoc comparisons showed significant differences between only on day 5 ($p = 0.05$) (Fig. 6 C).

On day 6, spatial memory retention was assessed in a probe trial. Compared with α-Gal A (+/0) controls, α-Gal A (−/0) mice spent less time in the former platform zone (time in quadrant α-Gal A (−/0) = 18.30 ± 1.964 α-Gal A (+/0) = 24.79 ± 1.431; two-tailed unpaired Student's *t*-test $t = 2.671$, df = 26, $p = 0.0129$; Fig. 6 D), higher Gallagher proximity score (α-Gal A (−/0) = 38.48 ± 2.461 α-Gal A (+/0) = 28.54 ± 1.196; two-tailed unpaired Student's t-test $t = 3.693$, df = 26, $p =$

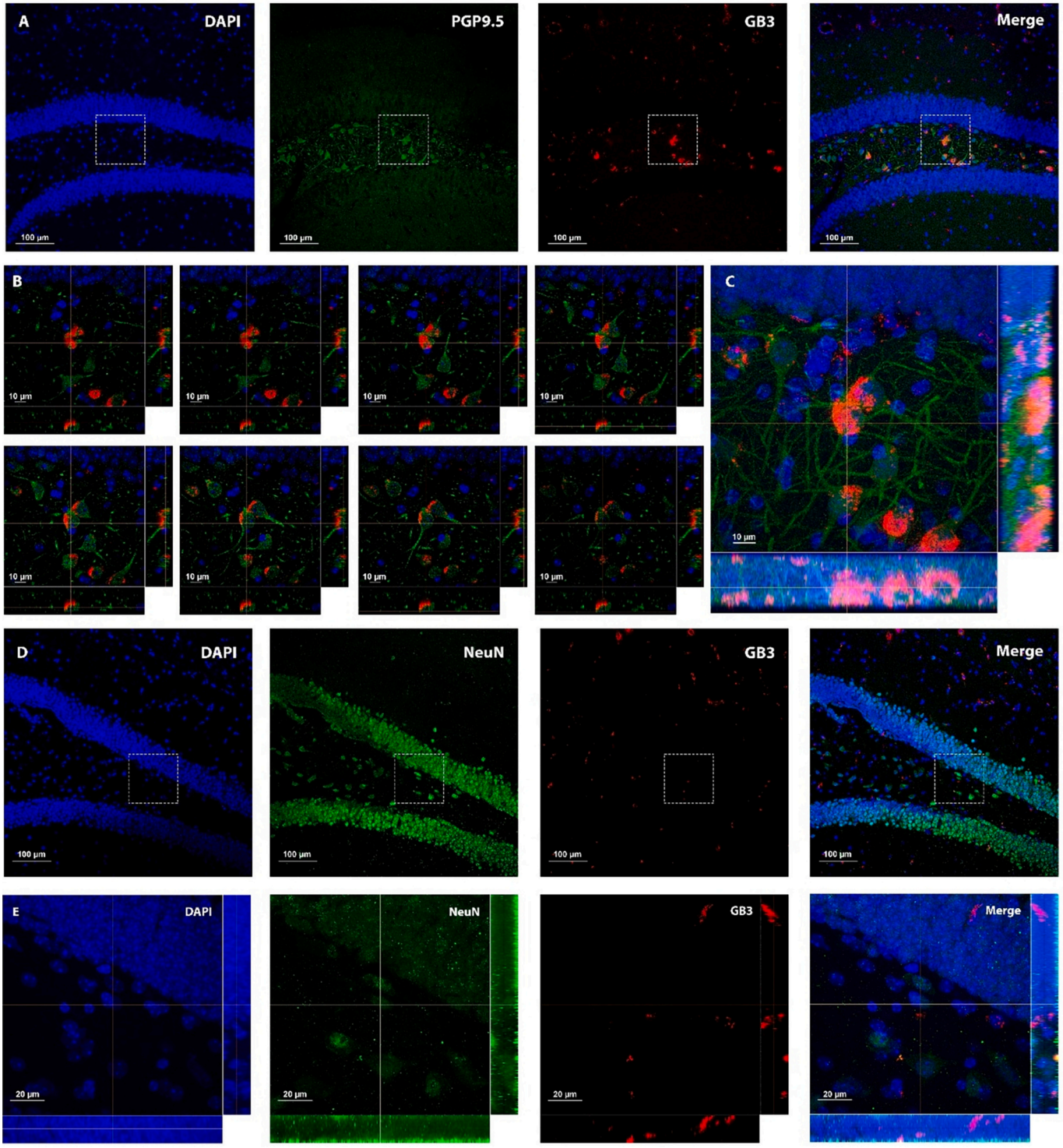

Fig. 2. Gb3-positive immunoreactivity is associated with neuronal somata. Neurons were labeled using PGP9.5 (A, B, C) and NeuN (D, E) antibodies. A: hippocampal coronal section of a α-Gal A (−/0) mouse stained for DAPI (Blue), PGP9.5 (green), Gb3 (red) and merged fluorescent signals (Merge), 20× magnification. B: high magnification (100×) of the region indicated by the white square in A. Images show several sequential focal planes of the region. The cross was pointed to a Gb3 immunoreactivity (red) in order to follow and show its position inside the neurons through the focal planes. C: maximum intensity projection of the fluorescent signals through the acquired z-scan focal planes of the white square region in A and in B, 100× magnification. D: hippocampal coronal section of a α-Gal A (−/0) mouse stained for DAPI (Blue), NeuN (green), Gb3 (red) and merged fluorescent signals (Merge), 20× magnification. E: high magnification (100×) of the region indicated by the white square in D. Images show, for each channel, the maximum intensity projection of the fluorescent signals through the acquired Z-scan focal planes of the white square region in D. Scale bars are indicated in the images. (α-Gal A (−/0): n = 6; 2–3 sections per animal). (For interpretation of the references to colour in this figure legend, the reader is referred to the web version of this article.)

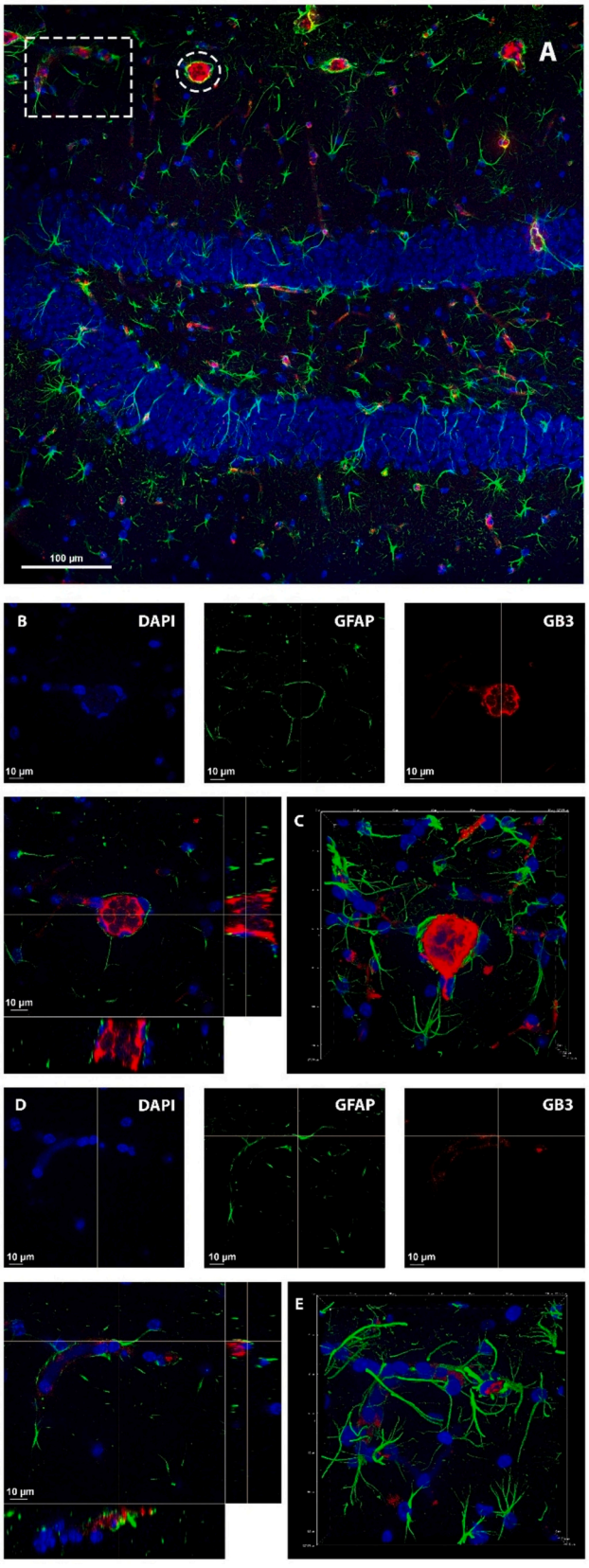

Fig. 3. Gb3 localization in astrocytes. A. Coronal section of the hippocampus of a α-Gal A (−/0) mice stained for GFAP (green) and Gb3 (red) (20× magnification). Accumulation of Gb3 can be observed inside cerebral capillaries surrounded by GFAP-positive astrocytes (rectangle and circle white regions in A). The following images (B-E) show these regions taken at high magnification (100×). The circle region (B—C) shows a coronal section of a blood vessel marked for DAPI (blue), GFAP (green), and Gb3 (red). No overlapping between Gb3 and GFAP signal can be observed in the YZ and XZ axis of the merged image (merge) or in the three-dimensional reconstruction of the vessel (C). Similar observations can be made for the longitudinal section of a blood vessel recognizable in the rectangle region in A, and showed at high magnification in D and E. Scale bars are indicated in the images. (α-Gal A (−/0): n = 6; 2–3 sections per animal). (For interpretation of the references to colour in this figure legend, the reader is referred to the web version of this article.)

0.001; Fig. 6 E), increased latency to enter former platform quadrant (α-Gal A (−/0) = 10.29 ± 2.422 α-Gal A (+/0) = 2.737 ± 0.347; two-tailed unpaired Student's t-test $t = 3.088$, df = 26, $p = 0.0047$; Fig. 6 F) and a decrease frequency in former platform crossing (α-Gal A (−/0) = 3 ± 0.52 α-Gal A (+/0) = 6 ± 0.17; two-tailed unpaired Student's t-test $t = 3.2$, df = 26, $p = 0.0036$; Fig. 6 G. No significant genotype differences were observed for total swimming distance (α-Gal A (−/0) = 1448 ± 61.3 α-Gal A (+/0) = 1545 ± 31.93; two-tailed unpaired Student's t-test $t = 1.415$, df = 26, $p = 0.682$; Fig. 6 H) or swimming speed (α-Gal A (−/0) = 23.45 ± 1.14 α-Gal A (+/0) = 25.88 ± 0.55; two-tailed unpaired Student's t-test $t = 1.895$, df = 26, $p = 0.07$; Fig. 6 I).

4. Discussion

The present study provides convergent anatomical and behavioral evidence for hippocampal involvement in the α -Gal A (−/0) mouse model of FD. Using immunofluorescence and confocal microscopy, we detected an increase in hippocampal Gb3 immunoreactivity in knockout mice compared with wild-type controls, with Gb3-positive structures localized predominantly to hippocampal microvessels and, more selectively, to dentate gyrus hilar neurons with mossy cell-like morphology. Functionally, α -Gal A (−/0) mice displayed impaired spatial learning and reduced memory retention in the MWM in the absence of gross motor confounds. Together, these findings support the hypothesis that α -Gal A deficiency could promote hippocampal substrate deposition and is associated with measurable cognitive impairment.

The hippocampus was selected because it is essential for spatial learning and memory information processing (Amaral et al., 2007; Vorhees and Williams, 2006). In FD, cognitive symptoms are usually interpreted in relation to cerebrovascular disease, white matter injury, pain burden, mood disturbance, and systemic disease severity (Bolsover et al., 2014; Loeb et al., 2018; Mroczek et al., 2022). However, whether local hippocampal substrate deposition contributes to hippocampus-dependent behavioral impairment remains unclear. The combination of hippocampal Gb3 immunoreactivity and MWM impairment in the present study therefore provides an anatomical and functional rationale for using this model to investigate neurovascular contributions to cognitive vulnerability in FD.

A major implication of our data is the predominance of a neurovascular storage pattern. The present observation is in line with previous reports showing CNS involvement in FD is mainly at vascular level with or without regionally restricted parenchymal changes. In FD patients, central nervous system manifestations are linked to cerebral small-vessel disease, white matter abnormalities, lacunar infarcts, altered cerebral perfusion and stroke risk (Buechner et al., 2008; Hilz et al., 2004; Mitsias and Levine, 1996; Moore et al., 2007). Neuropathological and neuroimaging studies have highlighted preferential glycosphingolipid deposition within vascular compartments, particularly endothelial cells, with downstream effects on vascular reactivity, while evidence for neuronal and glial storage is controversial and appears to depend on disease stage, tissue region and detection methods (Fellgiebel et al., 2012; Kaye et al.,

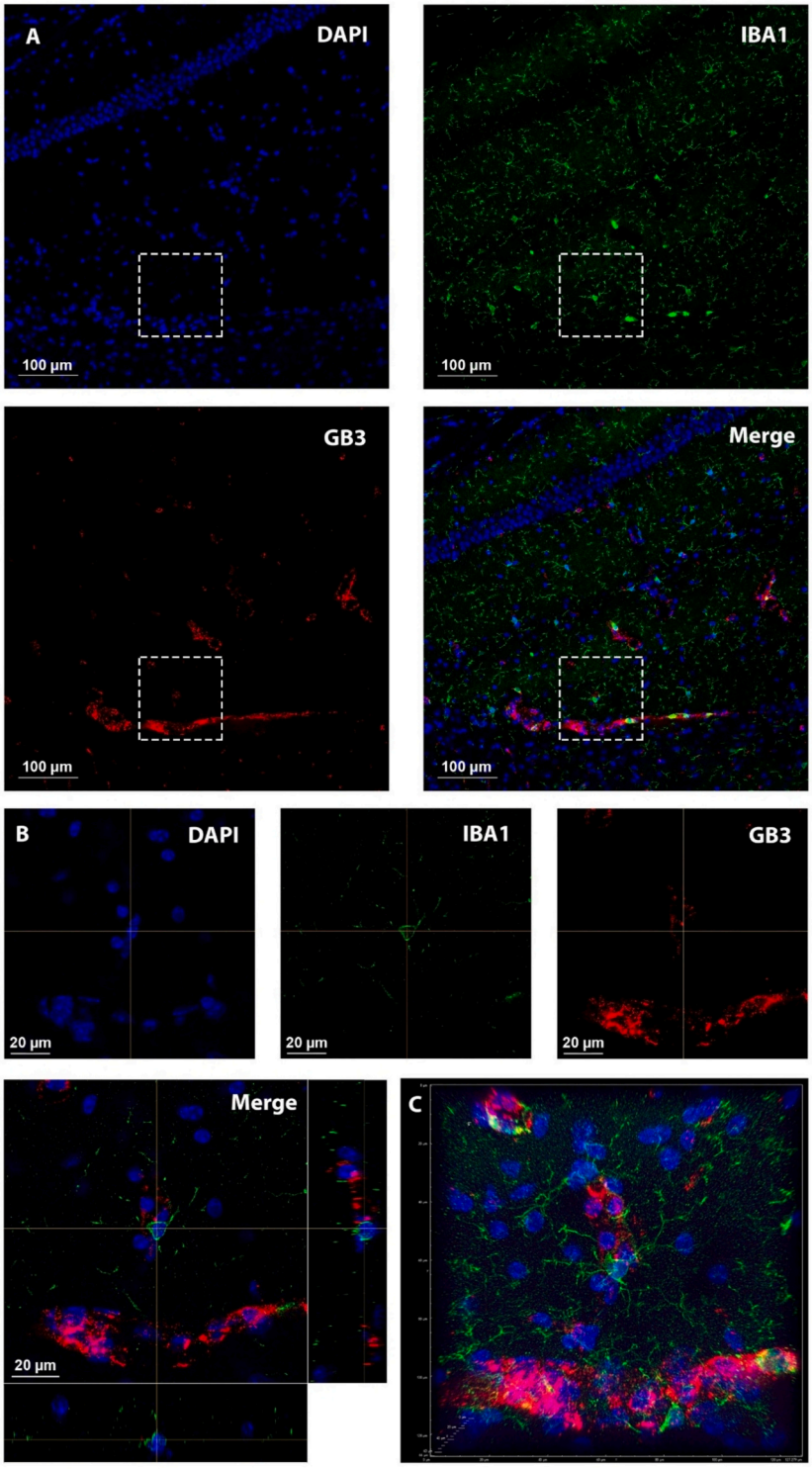

Fig. 4. Gb3 localization in microglia. A. Coronal section of the hippocampus of a α-GAL A (−/0) mice stained for Iba1 (green) and Gb3 (red) (20× magnification). Several Iba1-positive glial cells are present, while Gb3 immunoreactivity can be observed inside cerebral capillaries. B: high magnification (100×) of the region indicated by the white square in A. Images show a single focal plane of the region. The cross was pointed to an Iba1-immunoreactive green cell in order to show the position of its soma and process in relation to a nearby Gb3 immunoreactivity. No colocalization between Gb3 and Iba1 signal can be observed in the YZ and XZ axis of the merged image (merge) or in the three-dimensional reconstruction of region (C). Scale bars are indicated in the images. (α-GAL A (−/0): n = 6; 2–3 sections per animal). (For interpretation of the references to colour in this figure legend, the reader is referred to the web version of this article.)

1988; Pontillo et al., 2024; Zedde et al., 2024). Mechanistically, glycosphingolipid accumulation has been associated with endothelial dysfunction, oxidative stress, and impaired autophagy/lysosomal pathways (Chévrier et al., 2010; Ludlaim et al., 2025; Tuttolomondo et al., 2024), processes that can compromise blood-brain barrier integrity and neurovascular coupling.

With regards to animal models, previous studies have indicated that the original α-Gal A knockout mouse line displays altered cerebral blood

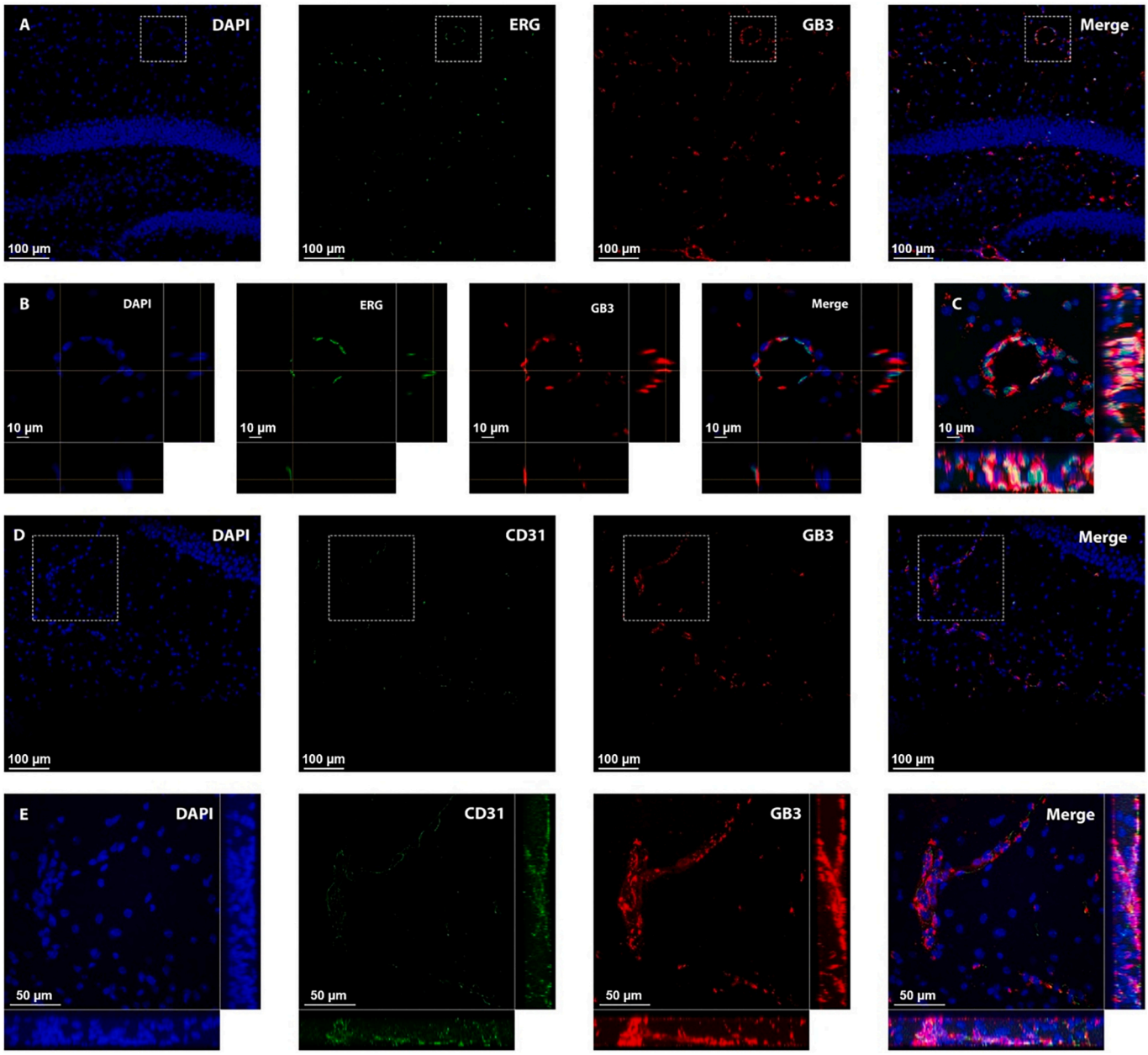

Fig. 5. Gb3 localization in cerebral vessels. Gb3 immunoreactivity in hippocampal vasculature was investigated through immunodetection of endothelial cells in the brain vessels using antibodies against ERG (A, B, C) and CD31 proteins (D, E). The representative fields shown correspond to the hippocampal subregion indicated in the low-magnification panel; vascular-associated Gb3 signal is shown as a hippocampal microvascular finding and should not be interpreted as dentate gyrus-specific neuronal localization. A: hippocampal coronal section of a α-GAL A (−/0) mouse stained for DAPI (Blue), ERG (green), Gb3 (red) and merged fluorescent signals (Merge), 20× magnification. B: higher magnification (100×) of the region indicated by the white square in A. Images show a single focal plane of the region. The cross was pointed to a Gb3 immunoreactivity (red) in order to show its position in space in relation to the ERG-positive nucleus (blue, green, merge) of an endothelial cell of the vessel. C: maximum intensity projection of the fluorescent signals through the acquired z-scan focal planes of the white square region in A and in B, 100× magnification. D: hippocampal coronal section of a α-GAL A (−/0) mouse stained for DAPI (Blue), CD31 (green), Gb3 (red) and merged fluorescent signals (Merge), 20× magnification. E: maximum intensity projection of the fluorescent signals through the acquired Z-scan focal planes of the white square region in D, 60× magnification. Scale bars are indicated in the images. (α-GAL A (−/0): n = 6; 2–3 sections per animal). (For interpretation of the references to colour in this figure legend, the reader is referred to the web version of this article.)

flow and glucose utilization, along with vascular wall deposits and limited neuronal involvement suggesting a primarily neurovascular phenotype (Itoh et al., 2001). Conversely, animal models exhibiting enhanced Gb3 synthesis or greater substrate burden demonstrate broader glycosphingolipid accumulation and more pronounced CNS alterations (Jabbarzadeh-Tabrizi et al., 2020; Taguchi et al., 2023, 2013).

Our observations are in line with the above-mentioned evidence since our results show that Gb3-positive structures surrounded ERG-positive endothelial nuclei and followed CD31-positive vessel walls without nuclear colocalization, consistent with cytoplasmic/organellar storage. The frequent detection of Gb3 immunoreactivity within the capillary lumen further suggests that substrate-related material may be present intravascularly, potentially reflecting endothelial release, impaired clearance, or circulating complexes (Lertkiatmongl et al., 2016). Although the current study does not directly measure perfusion or barrier permeability, the anatomical pattern is compatible with the notion that neurovascular dysfunction is a proximal driver of

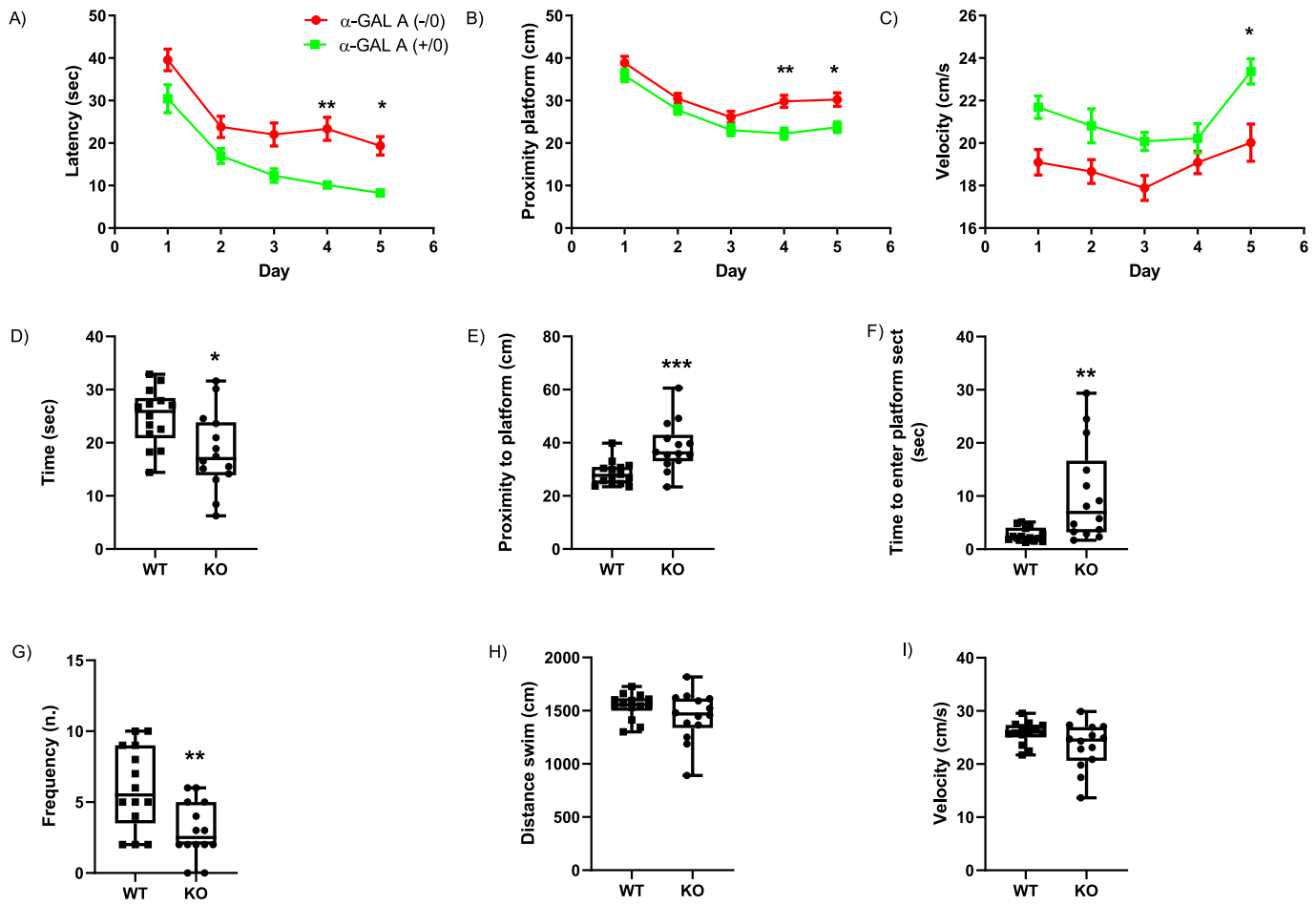

Fig. 6. Effects of α-Gal A deficiency on spatial learning and memory in the Morris water maze. A–C: Learning phase of the MWM evaluated as latency to reach the platform (A), swim proximity to platform (B), swim velocity (C) Values represent mean ± SEM. Data were analyzed by repeated-measures two-way ANOVA followed by Tukey HSD's post hoc tests * $p = 0.02$; ***$p = 0.0002$ vs α-Gal A (+/0); $n = 14$ each genotype. D-I: Spatial memory was assessed in the probe test after spatial learning. In the probe test, memory was assessed as time spent in former platform quadrant (D), proximity to the former platform (E), latency to reach the former platform (F), number of crossings (frequency) over the former platform (G), swimming total distance during probe test (H), swimming speed during the probe test (I). Box edges represent the 75th and 25th percentiles, median lines indicate the median, whiskers show the extreme values, circles and squares denote individual animals. * $p = 0.01$; ***$p = 0.001$; **$p \leq 0.001$ vs α-Gal A (+/0). Data (n = 14 each genotype) were analyzed by repeated-measures two-way ANOVA followed by Tukey HSD's post hoc tests; probe-trial variables were analyzed using two-tailed unpaired Student's *t*-tests.

hippocampal network stress in FD. It is important to note that the present immunofluorescence approach is unable to determine whether neuronal Gb3 signal reflects cell-autonomous neuronal glycosphingolipid accumulation or uptake of substrate-related material from adjacent vascular or perivascular compartments. This distinction is of particular relevance given that Gb3 and lyso-Gb3 are systemically circulating Fabry-related substrates (Celi et al., 2022; Nikolaenko et al., 2023; Ramaswami et al., 2025) and that the hippocampal signal observed here was predominantly neurovascular. Additional studies combining biochemical quantification, vascular permeability assays, and cell-type-specific approaches will be required to distinguish intrinsic neuronal storage from secondary uptake or perivascular accumulation.

Beyond the vasculature, we observed neuronal Gb3 signal restricted to hilar neurons with morphology consistent with mossy cells, a glutamatergic population that participates in dentate gyrus excitability and information gating (Amaral et al., 2007). Selective vulnerability of mossy cells could be particularly relevant for hippocampal-dependent computation, as perturbations at the dentate gyrus can impair spatial encoding and pattern separation. Our findings align with reports that neuronal Gb3 immunoreactivity can be detected in discrete brain regions in Fabry models (Itoh et al., 2001; Obata and Obrig, 2010) and support emerging evidence that hippocampal circuits may be affected in the disease. While we did not quantify hippocampal atrophy or synaptic markers, the combination of mossy cell-associated deposits and memory impairment suggests that even limited neuronal storage within a strategically placed population could amplify hippocampal dysfunction. However, it is important to be cautious when translating this neuronal finding to human FD. The evidence from human post-mortem studies indicates that the hippocampus is involved, although this evidence is limited and not fully consistent across reports. Kaye et al. (Kaye et al., 1988) described marked Gb3 accumulation in hippocampal structures, whereas Okeda and Nisihara (Okeda and Nisihara, 2008) reported neuronal hydropic swelling in the amygdaloid body and subiculum without clear dentate gyrus hilar involvement. Furthermore, reduced hippocampal volume has been reported in male Fabry patients without a direct correlation with significant memory loss, suggesting that age, disease stage, cognitive compensation, vascular burden, and phenotype heterogeneity may modulate the relationship between hippocampal pathology and clinical cognitive performance (Fellgiebel et al., 2012). On the contrary, neuroimaging studies have linked white matter integrity and network disconnection to cognitive performance (Gabusi et al., 2022; Johnson et al., 2025; Ulivi et al., 2021).

Glial analyses indicate that astrocytes and microglia are more likely responders than primary storage compartments in this model. We did not observe Gb3 positive signaling overlapping GFAP-positive astrocytes or Iba1-positive microglia, but astrocytic processes frequently wrapped

Gb3-positive capillaries and microglia displayed an activated morphology with processes oriented toward affected vessels. Similar dissociations between storage localization and inflammatory response have been proposed in Fabry pathogenesis, where vascular substrate accumulation and cellular stress can promote cytokine signaling and neuroinflammation without necessarily requiring glial substrate storage (Cortés-Saladelafont et al., 2023; Tuttolomondo et al., 2024). Given evidence that lysosomal dysfunction and impaired autophagy contribute broadly to neurodegeneration across lysosomal storage diseases (Chévrier et al., 2010; Ludlaim et al., 2025), future work should test whether neuroinflammatory pathways and glial-vascular signaling mediate hippocampal circuit disruption downstream of endothelial storage in α -Gal A (−/0) mice. It is noteworthy that Galimberti et al. (Galimberti et al., 2026) have recently shown the presence of severe and persistent neuroinflammation in the dorsal root ganglia of this animal FD model, characterized by the overexpression of prokineticin-2, proinflammatory cytokines, ionized calcium-binding adapter molecule 1 and glial fibrillary acidic protein.

Behaviorally, α -Gal A (−/0) mice showed slower acquisition and reduced probe-trial performance in the MWM consistent with a possible impaired hippocampal-dependent spatial learning and memory. These findings are relevant to clinical observations of cognitive complaints and deficits in FD, which have been reported in domains including processing speed, executive function, and memory, and are often discussed in the context of cerebrovascular burden and neuropsychiatric symptoms (Bolsover et al., 2014; Laney et al., 2010; Loeb et al., 2018; Mroczek et al., 2022; Ohsawa et al., 2024; Sigmundsdottir et al., 2014). Importantly, swimming speed and distance were not significantly different between genotypes, arguing against a primary motor explanation. Only limited behavioral work has been performed in this specific knockout line. Hofmann et al. reported no major genotype differences in water maze learning under their conditions (Hofmann et al., 2017), highlighting potential dependence on age, task parameters, and disease burden. Notably, our study focused on older mice (12–18 months), and paired behavior with hippocampal pathology, which may increase sensitivity to detect Fabry-related cognitive effects.

Our results also help reconcile the variability observed across Fabry mouse models. In the original α-Gal A knockout line, peripheral substrate storage and sensory ganglion pathology are prominent (Formaggio et al., 2022; Lakomá et al., 2016, 2014; Masotti et al., 2019; Obata, 2010), whereas central deposition has been inconsistently reported and, in some studies, interpreted as more consistent with later-onset Fabry phenotypes (Bangari et al., 2015). However, it should be noted that this mouse model does not differentiate between classic and late-onset FD phenotypes. Therefore, the endothelial-associated hippocampal microvascular Gb3 pattern observed here should be interpreted as a mechanistic feature of α-Gal A deficiency and may be most relevant to classic multisystem FD. When extrapolating to late-onset variants, however, greater caution is advised, as later-onset FD is typically linked to residual α-Gal A activity, more limited organ involvement, without significant vascular endothelial involvement (Bangari et al., 2015; Germain, 2010; Nance et al., 2006).

More recently, models that enhance Gb3 synthesis or combine genetic manipulations have demonstrated greater brain glycosphingolipid accumulation and hippocampal transcriptional and functional alterations, including anxiety-like behavior and altered hippocampal activity (Kummer et al., 2025, 2018; Taguchi et al., 2023, 2013). It should be noted that, recently, we have shown an anxiety-like behavior trait in α-Gal A (−/0) (Delprete et al., 2023). Within this context, our data provides a cellular-resolution anatomical bridge by demonstrating prominent hippocampal microvascular deposits with selective dentate gyrus neuronal involvement in the α -Gal A (−/0) model, together with a clear spatial memory phenotype. However, since the α-Gal A (−/0) mouse model does not reproduce the clinical distinction between classic and late-onset FD, the translational relevance of the endothelial phenotype observed here should be interpreted cautiously. In particular, the endothelial-associated Gb3 pattern may be more directly relevant to classic FD, whereas in late-onset forms vascular Gb3 deposition may be more restricted and may involve vascular smooth muscle cells rather than widespread endothelial compromise.

Several limitations should be considered. First, substrate quantification was based on immunoreactivity using a single anti-Gb3 antibody. Although α-Gal A (+/0) controls, parallel tissue processing, confocal *Z*-stack analysis, and multiple cell-type markers support the anatomical interpretation of the signal, immunofluorescence alone cannot establish the biochemical identity of all Gb3-positive structures with the same specificity as mass spectrometry. The present study also did not include staining for an additional lipid species as a control for generalized lipid accumulation or nonspecific lipid-associated signal. Second, we did not perform LC-MS/MS complementary biochemical measurements of Gb3 and lyso-Gb3 in microdissected hippocampus Such analysis would strengthen orthogonal validation since previous lipidomic studies in FD animal models have shown that Gb3 and lyso-Gb3 accumulation could vary by tissue, genotype and phenotype severity (Ishii et al., 2020; Jabbarzadeh-Tabrizi et al., 2020; Taguchi et al., 2023). Furthermore, it is important because lyso-Gb3 is used as a diagnostic and monitoring biomarker and there is increasing interest in its potential bioactivity (Nikolaenko et al., 2023; Ramaswami et al., 2025). Third, we studied cellular localization only in qualitative manner using confocal Z-stacks and orthogonal views rather than by independent antibody validation, lipidomics, electron microscopy, quantitative colocalization metrics or stereological quantification. For this reason, the localization data should be interpreted as evidence of Gb3 immunoreactivity associated with defined anatomical compartments, rather than as definitive biochemical proof of Gb3 storage in each cell type. Fourth, the present work did not directly assess vascular function, blood-brain barrier permeability, or cerebral blood flow, which are central to clinical CNS involvement (Cortés-Saladelafont et al., 2023; Hilz et al., 2004; Moore et al., 2007; Tuttolomondo et al., 2024). Fifth, the present anatomical analysis was restricted to selected hippocampal sections and did not systematically compare Gb3 burden across hippocampal subfields such as the dentate gyrus, CA1, and CA3, or across extrahippocampal regions with different vascular density and perfusion levels. Therefore, we are unable to determine whether Gb3 accumulation follows regional vascularization, blood-brain barrier properties, or watershed vulnerability. Sixth, although mice were analyzed at 12–18 months of age, the study was not powered to test age as an independent variable. It is therefore important to note that age-related differences in substrate accumulation may contribute to interindividual variability. This issue should be addressed in future age-stratified studies. Seventh, mechanistic links between storage, neuroinflammation, and synaptic/circuit dysfunction remain to be established. Future studies could combine in vivo imaging, vascular functional assays, electrophysiology, and expanded behavioral batteries to disentangle memory-specific effects from anxiety/depression-like phenotypes that have been reported in FD and models of the disease (Delprete et al., 2023; Kummer et al., 2025; Mroczek et al., 2022).

In conclusion, these findings indicate that α-Gal A deficiency is associated with increased hippocampal Gb3 immunoreactivity, predominantly in neurovascular compartments, and with impaired performance in a spatial navigation task consistent with hippocampal dysfunction. This neurovascular-dominant pattern mirrors key aspects of human CNS Fabry pathology characterized by cerebral small-vessel disease, altered perfusion and vascular substrate deposit (Buechner et al., 2008; Mitsias and Levine, 1996; Moore et al., 2007; Tuttolomondo et al., 2024). Furthermore, the present datasupports the utility of the α-Gal A (−/0) mouse as a platform to investigate neurovascular mechanisms contributing to cognitive dysfunction in FD. However, because Gb3 detection in the present study was based on immunofluorescence, future work should include orthogonal lipidomic validation, independent antibody confirmation, and functional assessment of neurovascular integrity.

Credit authorship contribution statement

Marco Salluzzo: Writing – review & editing, Writing – original draft, Methodology, Investigation, Formal analysis, Data curation, Conceptualization. **Francesca Flotta:** Writing – review & editing, Investigation, Data curation. **Cecilia Delprete:** Writing – review & editing, Methodology, Investigation, Formal analysis. **Violetta Lazzarotti:** Writing – review & editing, Investigation, Data curation. **Francesco Formaggio:** Writing – review & editing, Methodology, Data curation, Conceptualization. **Beatrice Vignoli:** Writing – review & editing, Methodology, Investigation, Formal analysis. **Ludovica Campolongo:** Writing – review & editing, Formal analysis. **Gabriele Campana:** Writing – review & editing, Formal analysis, Data curation. **Lucia Carboni:** Writing – review & editing, Funding acquisition. **Marco Canossa:** Writing – review & editing, Conceptualization. **Vincenzo Donadio:** Writing – review & editing. **Rocco Liguori:** Writing – review & editing, Funding acquisition. **Marco Caprini:** Writing – review & editing, Resources, Funding acquisition, Formal analysis, Data curation, Conceptualization. **Roberto Rimondini:** Writing – original draft, Methodology, Investigation, Funding acquisition, Formal analysis, Data curation, Conceptualization.

Declaration of competing interest

Authors declare that they have no known competing financial interests or personal relationships that could have appeared to influence the work reported in this paper.

Acknowledgement

The publication of this article was supported by a) the National Recovery and Resilience Plan (NRRP), project MNESYS (PE0000006) - "A multiscale integrated approach to the study of the nervous system in health and disease" (DN. 1553 11.10.2022) (RR); b) Fondazione Del Monte di Bologna ID ROL: FdM/4623 (MC), c) Fondazione Cassa di Risparmio in Bologna (2020.0404) (MC).

The publication of this article was supported by the "Ricerca Corrente" funding from the Italian Ministry of Health.

Appendix A. Supplementary data

Supplementary data to this article can be found online at https://doi.org/10.1016/j.nbd.2026.107516.

Data availability

Original data files will be made available to any qualified researcher through the online repository Zenodo.

References

Altarescu, G., Moore, D.F., Schiffmann, R., 2005. Effect of genetic modifiers on cerebral lesions in Fabry disease. Neurology 64, 2148–2150. https://doi.org/10.1212/01.WNL.0000166000.24321.4F.

Amaral, D.G., Scharfman, H.E., Lavenex, P., 2007. The dentate gyrus: fundamental neuroanatomical organization (dentate gyrus for dummies). Prog. Brain Res. 163, 3–22. https://doi.org/10.1016/S0079-6123(07)63001-5.

Bangari, D.S., Ashe, K.M., Desnick, R.J., Maloney, C., Lydon, J., Piepenhagen, P., Budman, E., Leonard, J.P., Cheng, S.H., Marshall, J., Thurberg, B.L., 2015. α-Galactosidase a knockout mice: progressive organ pathology resembles the type 2 later-onset phenotype of fabry disease. Am. J. Pathol. 185, 651–665. https://doi.org/10.1016/j.ajpath.2014.11.004.

Biegstraaten, M., Binder, A., Maag, R., Hollak, C.E.M., Baron, R., Van Schaik, I.N., 2011. The relation between small nerve fibre function, age, disease severity and pain in Fabry disease. Eur. J. Pain 15, 822–829. https://doi.org/10.1016/j.ejpain.2011.01.014.

Bolsover, F.E., Murphy, E., Cipolotti, L., Werring, D.J., Lachmann, R.H., 2014. Cognitive dysfunction and depression in Fabry disease: a systematic review. J. Inherit. Metab. Dis. https://doi.org/10.1007/s10545-013-9643-x.

Buechner, S., Moretti, M., Burlina, A.P., Cei, G., Manara, R., Ricci, R., Mignani, R., Parini, R., Di Vito, R., Giordano, G.P., Simonelli, P., Siciliano, G., Borsini, W., 2008. Central nervous system involvement in Anderson-Fabry disease: a clinical and MRI retrospective study. J. Neurol. Neurosurg. Psychiatry 79, 1249–1254. https://doi.org/10.1136/jnnp.2008.143693.

Celi, A.B., Goldstein, J., Rosato-Siri, M.V., Pinto, A., 2022. Role of globotriaosylceramide in physiology and pathology. Front. Mol. Biosci. https://doi.org/10.3389/fmolb.2022.813637.

Chévrier, M., Brakch, N., Lesueur, C., Genty, D., Ramdani, Y., Moll, S., Djavaheri-Mergny, M., Brasse-Lagnel, C., Laquerrière, A., Barbey, F., Bekri, S., 2010. Autophagosome maturation is impaired in Fabry disease. Autophagy 6, 589–599. https://doi.org/10.4161/auto.6.5.11943.

Cortés-Saladelafont, E., Fernández-Martín, J., Ortolano, S., 2023. Fabry disease and central nervous system involvement: from big to small, from brain to synapse. Int. J. Mol. Sci. https://doi.org/10.3390/ijms24065246.

Crutchfield, K.E., Patronas, N.J., Dambrosia, J.M., Frei, K.P., Banerjee, T.K., Barton, N. W., Schiffmann, R., 1998 Jun. Quantitative analysis of cerebral vasculopathy in patients with Fabry disease. Neurology 50 (6), 1746–1749. https://doi.org/10.1212/wnl.50.6.1746.

Delprete, C., Rimondini Giorgini, R., Lucarini, E., Bastiaanssen, T.F.S., Scicchitano, D., Interino, N., Formaggio, F., Uhlig, F., Ghelardini, C., Hyland, N.P., Cryan, J.F., Liguori, R., Candela, M., Fiori, J., Turroni, S., Di Cesare Mannelli, L., Caprini, M., 2023. Disruption of the microbiota-gut-brain axis is a defining characteristic of the α-gal a (−/0) mouse model of Fabry disease. Gut Microbes 15. https://doi.org/10.1080/19490976.2023.2256045.

Elsaid, H.O.A., Furriol, J., Blomqvist, M., Diswall, M., Leh, S., Gharbi, N., Anonsen, J.H., Babickova, J., Tøndel, C., Svarstad, E., Marti, H.P., Krause, M., 2022. Reduced α-galactosidase A activity in zebrafish (Danio rerio) mirrors distinct features of Fabry nephropathy phenotype. Mol. Genet. Metab. Rep. 31. https://doi.org/10.1016/j.ymgmr.2022.100851.

Faul, F., Erdfelder, E., Lang, A.-G., Buchner, A., 2007. Statistics textbooks in the. Behav. Res. Methods 39, 175–191.

Fellgiebel, A., Wolf, D.O., Kolodny, E., Müller, M.J., 2012. Hippocampal atrophy as a surrogate of neuronal involvement in Fabry disease. J. Inherit. Metab. Dis. 35, 363–367. https://doi.org/10.1007/s10545-011-9390-9.

Formaggio, F., Rimondini, R., Delprete, C., Scalia, L., Merlo Pich, E., Liguori, R., Nicoletti, F., Caprini, M., 2022. L-Acetylcarnitine causes analgesia in mice modeling Fabry disease by up-regulating type-2 metabotropic glutamate receptors. Mol. Pain 18. https://doi.org/10.1177/17448069221087033.

Gabusi, I., Pontillo, G., Petracca, M., Battocchio, M., Bosticardo, S., Costabile, T., Daducci, A., Pane, C., Riccio, E., Pisani, A., Brunetti, A., Schiavi, S., Cocozza, S., 2022. Structural disconnection and functional reorganization in Fabry disease: a multimodal MRI study. Brain Commun. 4. https://doi.org/10.1093/braincomms/fcac187.

Galimberti, G., Franchi, S., Amodeo, G., Romualdi, P., Candeletti, S., Rullo, L., Losapio, L. M., Onnis, V., Moi, D., Riboldi, B., Magni, G., Ceruti, S., Sacerdote, P., 2026. The prokineticin system and glia cells as pharmacological targets to control neuroinflammation and to relieve pain in a murine model of Fabry-Anderson disease. Pain 167, 428–442. https://doi.org/10.1097/j.pain.0000000000003818.

Germain, D.P., 2010. Fabry disease. Orphanet J. Rare Dis. https://doi.org/10.1186/1750-1172-5-30.

Grewal, R.R., Grewal, R.P., 1994. Stroke in Fabry's disease. J. Neurol. 241, 153–156. https://doi.org/10.1007/BF00868342.

Haber, M.A., Iranmahboob, A., Thomas, C., Liu, M., Najjar, A., Zagzag, D., 2015. ERG is a novel and reliable marker for endothelial cells in central nervous system tumors. Clin. Neuropathol. 34, 117–127. https://doi.org/10.5414/NP300817.

Hilz, M.J., Kolodny, E.H., Brys, M., Stemper, B., Haendl, T., Marthol, H., 2004. Reduced cerebral blood flow velocity and impaired cerebral autoregulation in patients with Fabry disease. J. Neurol. 251, 564–570. https://doi.org/10.1007/s00415-004-0364-9.

Hofmann, L., Karl, F., Sommer, C., Üçeyler, N., 2017. Affective and cognitive behavior in the alpha-galactosidase A deficient mouse model of Fabry disease. PLoS One 12. https://doi.org/10.1371/journal.pone.0180601.

Imai, Y., Ibata, I., Ito, D., Ohsawa, K., Kohsaka, S., 1996. A novel gene iba1 in the major histocompatibility complex class III region encoding an EF hand protein expressed in a monocytic lineage 1. Biochem. Biophys. Res. Commun. 224, 855–862. https://doi.org/10.1006/bbrc.1996.1112.

Ishii, S., Taguchi, A., Okino, N., Ito, M., Maruyama, H., 2020. Determination of globotriaosylceramide analogs in the organs of a mouse model of Fabry disease. J. Biol. Chem. 295, 5577–5587. https://doi.org/10.1074/jbc.RA120.012665.

Itoh, Y., Esaki, T., Cook, M., Qasba, P., Shimoji, K., Alroy, J., Brady, R.O., Sokoloff, L., Moore, D.F., 2001. Local and global cerebral blood flow and glucose utilization in the α-galactosidase a knockout mouse model of Fabry disease. J. Neurochem. 79, 1217–1224. https://doi.org/10.1046/j.1471-4159.2001.00669.x.

Jabbarzadeh-Tabrizi, S., Boutin, M., Day, T.S., Taroua, M., Schiffmann, R., Auray-Blais, C., Shen, J.S., 2020. Assessing the role of glycosphingolipids in the phenotype severity of Fabry disease mouse model. J. Lipid Res. 61, 1410–1423. https://doi.org/10.1194/jlr.RA120000909.

Johnson, J.W., Baradaran, H., Morgan, J., Odèen, H., Friel, E., Bailey, C., Zielinski, B.A., Underhill, H.R., 2025. The insidious degeneration of white matter and cognitive decline in Fabry disease. PLoS One 20, e0325403. https://doi.org/10.1371/journal.pone.0325403.

Juchniewicz, P., Kloska, A., Tylki-Szymańska, A., Jakóbkiewicz-Banecka, J., Węgrzyn, G., Moskot, M., Gabig-Cimińska, M., Piotrowska, E., 2018. Female Fabry disease patients and X-chromosome inactivation. Gene 641, 259–264. https://doi.org/10.1016/j.gene.2017.10.064.

Kaye, E.M., Kolodny, E.H., Logigian, E.L., David Ullman, M., 1988. Nervous system involvement in Fabry's disease: clinicopathological and biochemical correlation, 23, 505–509. https://doi.org/10.1002/ana.410230513.
Kummer, KK, Kalpachidou, T, Mitrić, M, Langeslag, M, Kress, M, 2018. Altered gene expression in prefrontal cortex of a fabry disease mouse model. Front Mol. Neurosci. 11, 201. https://doi.org/10.3389/fnmol.2018.00201.
Kummer, K., Choconta, J.L., Edenhofer, M.L., Bajpai, A., Dharmalingam, G., Kalpachidou, T., Collier, D.A., Kress, M., 2025. Anxiety-like behavior and altered hippocampal activity in a transgenic mouse model of Fabry disease. Neurobiol. Dis. 205. https://doi.org/10.1016/j.nbd.2025.106797.
Lakomá, J., Rimondini, R., Donadio, V., Liguori, R., Caprini, M., 2014. Pain related channels are differentially expressed in neuronal and non-neuronal cells of glabrous skin of fabry knockout male mice. PLoS One 9. https://doi.org/10.1371/journal.pone.0108641.
Lakomá, J., Rimondini, R., Montiel, A.F., Donadio, V., Liguori, R., Caprini, M., 2016. Increased expression of trpv1 in peripheral terminals mediates thermal nociception in fabry disease mouse model. Mol. Pain 12, 1–16. https://doi.org/10.1177/1744806916663729.
Laney, D.A., Gruskin, D.J., Fernhoff, P.M., Cubells, J.F., Ousley, O.Y., Hipp, H., Mehta, A. J., 2010. Social-adaptive and psychological functioning of patients affected by Fabry disease. J. Inherit. Metab. Dis. 33. https://doi.org/10.1007/s10545-009-9025-6.
Lidove, O., Klein, I., Lelièvre, J.D., Lavallée, P., Serfaty, J.M., Dupuis, E., Papo, T., Laissy, J.P., 2006. Imaging features of Fabry disease. Am. J. Roentgenol. 186, 1184–1191. https://doi.org/10.2214/AJR.05.0019.
Loeb, J., Feldt-Rasmussen, U., Madsen, C.V., Vogel, A., 2018. Cognitive Impairments and Subjective Cognitive Complaints in Fabry Disease: A Nationwide Study and Review of the Literature. In: JIMD Reports. Springer, pp. 73–80. https://doi.org/10.1007/8904_2018_103.
Ludlaim, A.M., Waddington, S.N., McKay, T.R., 2025. Unifying biology of neurodegeneration in lysosomal storage diseases. J. Inherit. Metab. Dis. 48. https://doi.org/10.1002/jimd.12833.
Masotti, M., Delprete, C., Dothel, G., Donadio, V., Rimondini, R., Politei, J.M., Liguori, R., Caprini, M., 2019. Altered globotriaosylceramide accumulation and mucosal neuronal fiber density in the colon of the Fabry disease mouse model. Neurogastroenterol. Motil. 31. https://doi.org/10.1111/nmo.13529.
Miller, J.J., Aoki, K., Tiemeyer, M., Dahms, N.M., 2016. The α-galactosidase A-deficient rat: characterization of a new animal model of Fabry disease. Mol. Genet. Metab. 117. https://doi.org/10.1016/j.ymgme.2015.12.362.
Miller, J.J., Kanack, A.J., Dahms, N.M., 2020. Progress in the understanding and treatment of Fabry disease. Biochim. Biophys. Acta Gen. Subj. https://doi.org/10.1016/j.bbagen.2019.129437.
Mitsias, P., Levine, S.R., 1996. Cerebrovascular complications of Fabry's disease. Ann. Neurol. 40, 8–17. https://doi.org/10.1002/ana.410400105.
Moore, D.F., Altarescu, G., Ling, G.S.F., Jeffries, N., Frei, K.P., Weibel, T., Charria-Ortiz, G., Ferri, R., Arai, A.E., Brady, R.O., Schiffmann, R., 2002. Elevated cerebral blood flow velocities in Fabry disease with reversal after enzyme replacement. Stroke 33, 521–531. https://doi.org/10.1161/hs0202.102601.
Moore, D.F., Kaneski, C.R., Askari, H., Schiffmann, R., 2007. The cerebral vasculopathy of Fabry disease. J. Neurol. Sci. 257 (1–2), 258–263. https://doi.org/10.1016/j.jns.2007.01.053.
Mroczek, M., Maniscalco, I., Sendel, M., Baron, R., Seifritz, E., Nowak, A., 2022. Neuropsychiatric symptoms and their association with sex, age, and enzyme replacement therapy in Fabry disease: a systematic review. Front. Psychiatry. https://doi.org/10.3389/fpsyt.2022.829128.
Nance, C.S., Klein, C.J., Banikazemi, M., Dikman, S.H., Phelps, R.G., McArthur, J.C., Rodriguez, M., Desnick, R.J., 2006 Mar. Later-onset Fabry disease: an adult variant presenting with the cramp-fasciculation syndrome. Arch. Neurol. 63 (3), 453–457. https://doi.org/10.1001/archneur.63.3.453.
Nikolaenko, V., Warnock, D.G., Mills, K., Heywood, W.E., 2023. Elucidating the toxic effect and disease mechanisms associated with Lyso-Gb3 in Fabry disease. Hum. Mol. Genet. 32, 2464–2472. https://doi.org/10.1093/hmg/ddad073.
Obata, F., 2010. Influence of Escherichia coli Shiga toxin on the mammalian central nervous system. In: Advances in Applied Microbiology. Academic Press Inc., pp. 1–19. https://doi.org/10.1016/S0065-2164(10)71001-7
Obata, F., Obrig, T., 2010. Distribution of Gb 3 immunoreactivity in the mouse central nervous system. Toxins (Basel). 2, 1997–2006. https://doi.org/10.3390/toxins2081997.
Ohsawa, I., Onuki, A., Oka, F., Matsuoka, Y., Makita, Y., Kobayashi, T., Kanaguchi, Y., Nakamura, Y., Suzuki, Y., Goto, Y., Gotoh, H., 2024. Rapidly progressive cognitive impairment resulting in heavy psychosocial burden in a patient with Fabry disease undergoing hemodialysis: a case report. BMC Nephrol. 25. https://doi.org/10.1186/s12882-024-03624-9.
Ohshima, T., Murray, G.J., Swaim, W.D., Longenecker, G., Quirk, J.M., Cardarelli, C.O., Sugimoto, Y., Pastan, I., Gottesman, M.M., Brady, R.O., Kulkarni, A.B., 1997. α-Galactosidase A deficient mice: a model of fabry disease. Proc. Natl. Acad. Sci. USA 94. https://doi.org/10.1073/pnas.94.6.2540.
Okeda, R., Nisihara, M., 2008. An autopsy case of Fabry disease with neuropathological investigation of the pathogenesis of associated dementia. Neuropathology 28, 532–540. https://doi.org/10.1111/j.1440-1789.2008.00883.x.
Perrot, A., Osterziel, K.J., Beck, M., Dietz, R., Kampmann, C., 2002. Fabry disease: focus on cardiac manifestations and molecular mechanisms. Herz. https://doi.org/10.1007/s00059-002-2429-9.
Pontillo, G., Tranfa, M., Scaravilli, A., Monti, S., Capuano, I., Riccio, E., Rizzo, M., Brunetti, A., Palma, G., Pisani, A., Cocozza, S., 2024. In vivo demonstration of globotriaosylceramide brain accumulation in Fabry disease using MR relaxometry. Neuroradiology 66, 1593–1601. https://doi.org/10.1007/s00234-024-03380-5.
Ramaswami, U., West, M.L., Tylee, K., Castillon, G., Braun, A., Ren, M., Doobaree, I.U., Howitt, H., Nowak, A., 2025. The use and performance of lyso-Gb3 for the diagnosis and monitoring of Fabry disease: a systematic literature review. Mol. Genet. Metab. https://doi.org/10.1016/j.ymgme.2025.109110.
Ranieri, M., Bedini, G., Parati, E.A., Bersano, A., 2016. Fabry disease: recognition, diagnosis, and treatment of neurological features. Curr. Treat. Options Neurol. https://doi.org/10.1007/s11940-016-0414-5.
Rullo, L., Posa, L., Caputi, F.F., Stamatakos, S., Formaggio, F., Caprini, M., Liguori, R., Candeletti, S., Romualdi, P., 2021. Nociceptive behavior and central neuropeptidergic dysregulations in male and female mice of a Fabry disease animal model. Brain Res. Bull. 175, 158–167. https://doi.org/10.1016/j.brainresbull.2021.07.027.
Schindelin, J., Arganda-Carreras, I., Frise, E., Kaynig, V., Longair, M., Pietzsch, T., Preibisch, S., Rueden, C., Saalfeld, S., Schmid, B., Tinevez, J.Y., White, D.J., Hartenstein, V., Eliceiri, K., Tomancak, P., Cardona, A., 2012. Fiji: an open-source platform for biological-image analysis. Nat. Methods. https://doi.org/10.1038/nmeth.2019.
Sigmundsdottir, L., Tchan, M.C., Knopman, A.A., Menzies, G.C., Batchelor, J., Sillence, D. O., 2014. Cognitive and psychological functioning in Fabry disease. Arch. Clin. Neuropsychol. 29, 642–650. https://doi.org/10.1093/arclin/acu047.
Stagni, F., Giacomini, A., Emili, M., Trazzi, S., Guidi, S., Sassi, M., Ciani, E., Rimondini, R., Bartesaghi, R., 2016. Short- and long-term effects of neonatal pharmacotherapy with epigallocatechin-3-gallate on hippocampal development in the Ts65Dn mouse model of down syndrome. Neuroscience 333, 277–301. https://doi.org/10.1016/j.neuroscience.2016.07.031.
Sun, Y., Ip, P., Chakrabartty, A., 2017. Simple elimination of background fluorescence in formalin-fixed human brain tissue for immunofluorescence microscopy. J. Vis. Exp. https://doi.org/10.3791/56188.
Taguchi, A., Maruyama, H., Nameta, M., Yamamoto, T., Matsuda, J., Kulkarni, A.B., Yoshioka, H., Ishii, S., 2013. A symptomatic Fabry disease mouse model generated by inducing globotriaosylceramide synthesis. Biochem. J. 456, 373–383. https://doi.org/10.1042/BJ20130825.
Taguchi, A., Ishii, S., Mikame, M., Maruyama, H., 2023. Distinctive accumulation of globotriaosylceramide and globotriaosylsphingosine in a mouse model of classic Fabry disease. Mol. Genet. Metab. Rep. 34. https://doi.org/10.1016/j.ymgmr.2022.100952.
Tuttolomondo, A., Baglio, I., Riolo, R., Todaro, F., Parrinello, G., Miceli, S., Simonetta, I., 2024. Molecular pathogenesis of central and peripheral nervous system complications in Anderson–Fabry disease. Int. J. Mol. Sci. https://doi.org/10.3390/ijms25010061.
Ulivi, L., Kanber, B., Prados, F., Davagnanam, I., Merwick, A., Chan, E., Williams, F., Hughes, D., Murphy, E., Lachmann, R.H., Gandini Wheeler-Kingshott, C.A.M., Cipolotti, L., Werring, D.J., 2021. White matter integrity correlates with cognition and disease severity in Fabry disease. Brain 143, 3331–3342. https://doi.org/10.1093/BRAIN/AWAA282.
Vorhees, C.V., Williams, M.T., 2006. Morris water maze: procedures for assessing spatial and related forms of learning and memory. Nat. Protoc. 1, 848–858. https://doi.org/10.1038/nprot.2006.116.
Wallace, R.D., Cooper, W.J., 1965. Angiokeratoma corporis diffusum universale (Fabry). Am. J. Med. 39, 656–661. https://doi.org/10.1016/0002-9343(65)90086-0.
Zedde, M., Romani, I., Scaravilli, A., Cocozza, S., Trojano, L., Ragno, M., Rifino, N., Bersano, A., Gerevini, S., Pantoni, L., Valzania, F., Pascarella, R., 2024. Expanding the neurological phenotype of Anderson–Fabry disease: proof of concept for an extrapyramidal neurodegenerative pattern and comparison with monogenic vascular Parkinsonism. Cells. https://doi.org/10.3390/cells13131131.